

Jet speeds in wide angle tailed radio galaxies

Nazirah N. Jetha¹*, Martin J. Hardcastle², and Irini Sakelliou³

¹*School of Physics and Astronomy, University of Birmingham, Edgbaston, Birmingham B15 2TT*

²*School of Physics, Astronomy and Mathematics, University of Hertfordshire, College Lane, Hatfield, Hertfordshire AL10 9AB*

³*Max Planck Institut für Astronomie, Königstuhl 17, D-69117, Heidelberg*

5 November 2018

ABSTRACT

We present a sample of 30 wide angle tailed radio galaxies (WATs) that we use to constrain the jet speeds in these sources. We measure the distribution of jet-sidedness ratios for the sample, and assuming that the jets are beamed, jet speeds in the range (0.3–0.7)c are obtained. Whilst the core prominence of the sample, which ought to be a reliable indicator of beaming, shows little correlation with the jet-sidedness, we argue that due to the peculiar nature of WATs core-prominence is unlikely to be a good indicator of beaming in these sources. We further show that if the jets are fast and light, then the galaxy speeds required to bend jets into C-shapes such as those seen in 0647+693 are reasonable for a galaxy in a merging or recently merged cluster.

Key words: galaxies: active - galaxies: clusters - radio continuum: galaxies

1 INTRODUCTION

Usually classified as FRI sources (Fanaroff & Riley 1974), wide angle tailed radio galaxies (WATs) are now thought to be an interesting hybrid of both FRI and FRII morphologies; they exhibit well collimated inner jets, which flare suddenly into diffuse plumes. These jets, which typically extend for tens of kiloparsecs and often terminate in compact radio-bright features similar to the hotspots of FRII sources (Hardcastle & Sakelliou 2004), appear superficially similar to the longer jets seen in FRII sources, whereas the diffuse plumes resemble more those found in FRI sources. The causes of the sudden jet flaring have been explored in detail in Jetha et al. (2005), where we note that the transition from a cooler core of X-ray emitting gas to a hotter, extended intra-cluster medium (ICM) co-incides with the jet flaring. However, as noted in our conclusions, there is uncertainty as to the nature of the jets; FRII jets are in general tightly collimated, and have moderate to high jet speeds (e.g. Hardcastle et al. 1999), whereas FRI jets tend to have large opening angles and also tend to be slower than FRII jets (e.g. Laing et al. 1999). Whilst jets in WATs superficially look like those of FRII sources, in that WAT jets tend to be well collimated, and have polarisation structures that resemble those found in FRII sources (Hardcastle & Sakelliou 2004), it is unclear whether their speeds resemble those of FRII sources or FRI sources. Establishing the nature of the WAT jets would allow us to establish whether WATs are failed FRIIs (Hardcastle 1999), or if they are a different sort of radio source altogether. Further, understanding the nature of the jets may help to explain the dynamics of the jets in clusters, in particular why the jets flare suddenly, and the relationship between jet length and the cluster environment.

The question of WAT jet speeds has been investigated before by O'Donoghue et al. (1990), who use a Monte Carlo analysis of a sample of 10 WAT sources to obtain a jet speed of 0.2c. Hardcastle & Sakelliou (2004) also address the issue of speeds in WAT jets, and obtain jet speeds of 0.3c. In both cases, the sources chosen for the samples investigated tend to exhibit two sided jets and this may have biased the results in the direction of reduced beaming effects and lower jet speeds.

In this paper, we use a larger sample of WATs, drawn from the catalogue of Abell clusters of Owen & Ledlow (1997), to better constrain the jet speed in WATs. We describe our sample selection procedure and data in Section 2; in Section 3, we discuss how we infer jet speeds from our data, and the speeds inferred; and in Section 4, we discuss the implications of this result. Throughout the paper, we assume that $H_0=70 \text{ km s}^{-1} \text{ Mpc}^{-1}$ and use J2000 co-ordinates.

2 SAMPLE SELECTION AND OBSERVATIONS

An initial sample of 67 sources was selected from the maps of the Owen & Ledlow (1997) 21-cm survey of Abell clusters. Our selection criteria were that a source had to be included in the Owen & Ledlow (1997) sample, and that there had to be evidence of the possibility of there being two well collimated jets, which was inferred from the existence of two bright plume bases aligned with the core, and lying approximately equidistant from the core. Sources with very one-sided jets were not excluded from the sample, and no account was taken of the distance of the source from the cluster centre. Sources where the inner jets are very bent, like 0647+693 (see Hardcastle & Sakelliou 2004) were not excluded from the sample. Well known WAT objects, such as Hydra A, which

* Email: nnj@star.sr.bham.ac.uk

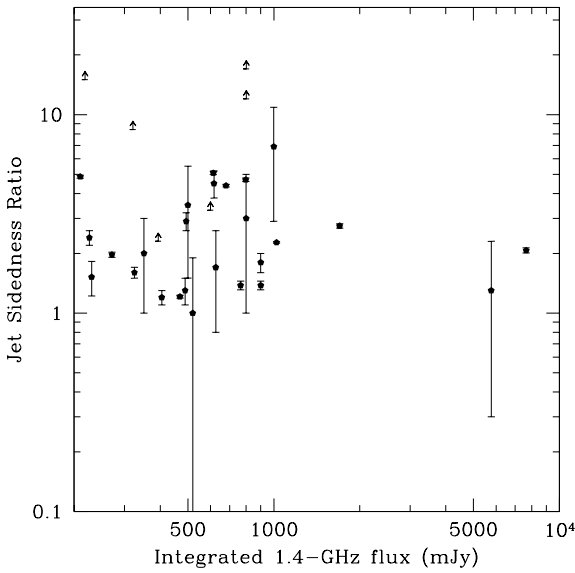


Figure 1. The jet sidedness ratios of the sources in our sample plotted against S_{1400} (taken from Owen & Ledlow 1997). The filled points represent actual jet detections, whilst the arrows show lower limits on the sidedness ratio.

were excluded from the Owen & Ledlow (1997) sample, were also excluded from this sample to keep our sample homogeneous.

The VLA data archive was then searched for high frequency, high resolution data for the sample objects. In cases where no archival data of the quality required were available, 8-GHz VLA observations were requested, and the sources were observed as part of this study. Those sources are marked in Table 1, and details of these observations and unpublished radio maps, both from the new observations and archival data, are presented in Appendix A. None of the radio sources observed by ourselves was excluded from the WAT sample; they all exhibited WAT morphology; however, two of the sources were excluded from this analysis, as the jets were not detected.

The data for all 67 candidate sources (both archival and our own observations) were reduced in AIPS in the standard way. After examination of the more detailed images provided by this process, sources that did not exhibit WAT morphology were excluded from the sample. We excluded 33 sources from the sample for this reason, and a further 4 (including the two from our own observations) were excluded from this analysis due to there not being enough information in the current maps to define the straight parts of the jets, resulting in a sample of 30 sources, which is presented in Table 1 and Fig 1. For each source the core flux was measured using the AIPS task JMFIT. The jet and counter-jet fluxes, which form the basis of the jet speed estimate, were also measured, using a combination of AIPS scripts that rotate the radio image so that the jets are horizontal, and allow the straight part of the jet and corresponding counter-jet regions to be defined, before the flux in those regions is measured, and corrected for the background. An error for the jet/counter-jet ratio was calculated by estimating the off source noise (in mJy/beam) for the jet and counter-jet, and multiplying by the square root of the number of beams in the jet and counter-jet regions. The errors on the jet and counter-jet fluxes were then combined together in the usual way to obtain an error on the jet/counter-jet ratio.

3 ESTIMATING THE JET SPEED AND MODELLING INTRINSIC SIDEDNESS

The jet part of the radio source can be modelled as two anti-parallel streams of plasma being emitted from the core of the radio source. The jets are inclined at some random angle θ to the line of sight; one jet travels towards the observer, the other travels away from the observer. Since the bulk velocity of the jet is relativistic, the flux of the jet moving towards us will be brightened via Doppler boosting, whereas the jet moving away from the observer will have its flux suppressed by a similar mechanism.

For a jet travelling at a speed $v = \beta c$, the relationship between the rest frame flux $S_0(\nu)$ and the Doppler boosted observed flux, $S(\nu)$ is given by

$$S(\nu) = S_0(\nu) [\gamma(1 - \beta \cos \theta)]^{-(2+\alpha)} \quad (1)$$

where γ is the Lorentz factor, $\gamma = (1 - \beta^2)^{-1/2}$.

Since Eqn. 1 can be applied equally to the jet and counter-jet, the jet/counter-jet ratio R , for a single source can place a constraint on $\beta \cos \theta$. R is given by (Lind & Blandford 1985):

$$R = k \left(\frac{1 + \beta \cos \theta}{1 - \beta \cos \theta} \right)^{-(2+\alpha)} \quad (2)$$

Here, k is the ratio between the rest frame jet and counter-jet flux; it is generally thought to be approximately unity, but can be varied to represent intrinsic variations in jet sidedness. The spectral index α is a measure of how the flux of the jet varies with frequency, and is defined such that $S(\nu) \propto \nu^{-\alpha}$. For the jets that are being dealt with here, we take $\alpha = 0.5$.

Assuming that the sources are randomly distributed over θ , a model distribution of R can be generated for given values of β and k , which can be compared with the observed distribution to obtain the most likely value for β in WATs.

We use a Monte Carlo technique to generate a distribution of jet sidedness ratios for given values of β and parameters affecting the intrinsic sidedness. This is then compared with the observed distribution to determine the values of the input parameters that maximize the likelihood. Rather than sampling a grid over all of parameter space, which can be computationally intensive, we use a Markov-Chain Monte Carlo (MCMC) algorithm to choose the model parameters to investigate. The implementation of the MCMC algorithm is the METRO sampler discussed by Hobson & Baldwin (2004), kindly provided by Mike Hobson. After an initial burn-in period to allow the Markov chain to converge, sets of model parameters are drawn from the chain, so that the highest-likelihood regions of parameter space are also the best sampled. The use of this algorithm to determine jet speeds will be discussed in more detail by Mullin et al. (prep).

It is usually assumed that there is no intrinsic difference between the two jets, i.e. k is unity. However, the physical conditions in both jet and counter-jet are unlikely to be identical, and this will lead to some intrinsic sidedness between the jet and counter-jet. Initially, we consider the case where the jet and counter-jet are symmetrical, and constrain the beaming speed β on the assumption that all of the observed sidedness distribution can be explained by beaming. We then relax this assumption, and simulate the case where some intrinsic asymmetry exists between the jet and counter-jet.

Our simulated sidedness data are constructed by generating different samples of jet/counter-jet pairs, with each sample having a different β , and equal rest frame fluxes for each jet/counter-jet pair. The angle that the jets make with the line of sight, θ is generated

Table 1. Details of the sources in our sample

Abell cluster	radio name (B1950)	z	S_{1400} (/ mJy)	obs. frequency (GHz)	core flux (mJy)	jet flux ¹ (mJy)	counter-jet flux ¹ (mJy)	jet/counter-jet flux ratio
A98	0043+201	0.11	900	4.8	12.3 ± 0.04	2.30	1.67	1.38 ± 0.07
A160	0110+152	0.045	1000	4.8	8.19 ± 0.05	2.02	0.293	6.9 ± 4
A194	3C40	0.018	5770	4.8	89.7 ± 0.08	4.59	3.67	1.3 ± 1
A562	0647+693	0.11	800	8.5	4.81 ± 0.03	0.518	0.172	3.0 ± 2
A595	0745+521	0.068	520	4.8	8.2 ± 0.2	2.60	2.55	1.0 ± 0.9
A610 [†]	0756+272	0.096	493	8.5	4.62 ± 0.02	6.37	2.18	2.9 ± 0.3
A690	0836+290	0.079	1022	4.8	137 ± 0.05	21.4	0.311	2.27 ± 0.02
A761	0908-102	0.092	177	4.8	8.90 ± 0.07	5.61	0.203	28 ± 2
A763	0909+162	0.085	183	4.8	1.13 ± 0.06	1.54	0.196	7.84 ± 2
A950 [†]	1011+500	0.21	394	8.5	41.0 ± 0.1	0.202	<0.0880	$>2.3 \pm 0.3$
A1238	1120+013	0.072	230	1.4	4.4 ± 0.4	2.00	1.31	1.52 ± 0.3
A1346*	1138+060	0.097	469	1.4	-	3.49	2.89	1.21 ± 0.02
A1446	1159+583	0.10	765	4.8	7.74 ± 0.04	3.51	2.54	1.38 ± 0.07
A1462 [†]	1202+153	0.14	614	8.5	-	39.5	7.77	5.08 ± 0.1
A1529 [†]	1221+615	0.23	321	8.5	15.9 ± 0.1	4.94	<0.587	$>8.42 \pm 0.08$
A1559	1231+674	0.11	900	8.5	5.41 ± 0.01	2.65	1.49	1.8 ± 0.2
A1684	1306+107A	0.086	405	4.8	6.42 ± 0.03	9.61	0.172	1.2 ± 0.1
A1763	1333+412	0.23	797	8.5	3.23 ± 0.01	5.07	1.09	4.7 ± 0.1
A1940	1433+553	0.14	500	8.5	14.97 ± 0.01	1.70	0.620	3.5 ± 2
A1942	1435+038	0.22	801	4.8	4.3 ± 0.1	4.77	<0.280	$>17 \pm 3$
A2029	1508+059	0.077	489	8.5	2.78 ± 0.01	1.10	0.878	1.3 ± 0.2
A2214	1636+379	0.16	617	4.8	6.78 ± 0.06	6.06	1.36	4.5 ± 0.7
A2220	1638+538	0.11	626	1.4	10.1 ± 0.5	5.08	2.97	1.7 ± 0.9
A2249 [†]	1707+344	0.081	680	8.5	6.37 ± 0.07	16.3	3.72	4.39 ± 0.06
A2304	1820+689	0.088	801	1.4	55.8 ± 0.3	7.00	<0.599	$>12 \pm 3$
A2306	1826+747	0.13	600	4.8	1.52 ± 0.04	0.262	<0.0792	$>3.3 \pm 0.3$
A2372	2142-202	0.058	351	4.8	0.9 ± 0.1	0.270	0.170	2 ± 1
A2395 [†]	2152+085	0.15	226	8.5	5.79 ± 0.03	3.91	1.62	2.4 ± 0.2
A2462	2236-176	0.073	1700	8.5	11.11 ± 0.02	17.9	6.52	2.75 ± 0.07
A2634	3C465	0.030	7650	8.5	213.49 ± 0.03	28.3	13.8	2.07 ± 0.06

NOTES: *We were unable to detect the core. ¹The jet and counter-jet fluxes were measured at 8.5 GHz. When measurements at 8.5 GHz were not available, measurements were made at other frequencies, and values for the jet fluxes were corrected assuming $\alpha=0.5$ and $S(\nu) \propto \nu^{-\alpha}$. Redshifts and 1.4 GHz fluxes were obtained from Ledlow & Owen (1995), and Owen & Ledlow (1997) respectively, except for the flux of 3C40, which was measured from our new radio map. Sources marked with a [†] were new observations for the purposes of this study.

randomly, in line with our assumption that there is no preferential angle. As can be seen from Table 1, some of our sample have only lower limits on the jet sidedness. This is taken into account in the fitting code by assigning a likelihood to the limit, such that the data point could take any value of sidedness in the parameter space that is greater than the limit. When intrinsic sidedness is introduced, each jet and counter-jet in a given sample has a different rest frame flux, but the same β . The rest frame flux is drawn from a truncated Gaussian distribution, centred on unity, and the width of the distribution (σ) is determined from the data. Thus, k is determined from the ratio of two truncated Gaussian distributions. The beamed sidedness distribution that is generated is then compared with the actual data, using a maximum likelihood method to determine which simulated sample best matches the observed distribution.

3.1 Modelling jets with beaming only

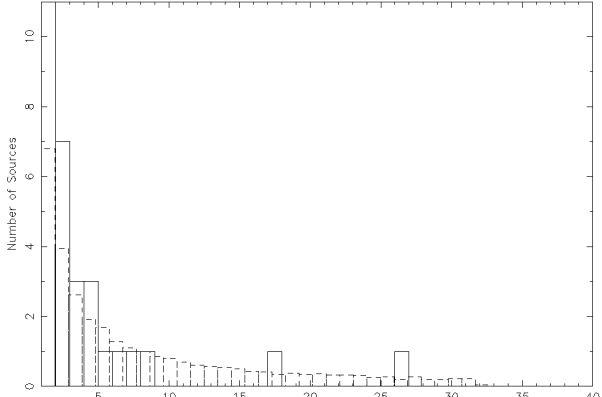
We initially modelled the case that the sidedness distribution was caused by beaming alone. The width of the Gaussian describing the intrinsic sidedness was set to zero, such that k in Eqn. 1 was unity. This gave a value of jet speed that created a sample which best matched the observed distribution. This jet speed was then used to generate synthetic samples firstly in order to act as a check that the

code was fitting the observed distribution correctly, and secondly to obtain a measure of the dispersion in the obtained value of the jet speed, which gives us an estimate of the uncertainty on the fitted parameters.

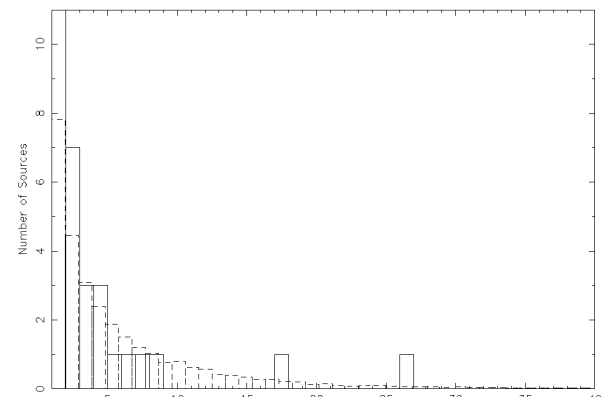
Using this method, a mean jet speed and dispersion of $\beta = 0.60 \pm 0.02$ was obtained for simulated data samples obtained as described above, assuming that beaming is the sole determinant of the observed sidedness distribution, and that the jet speed found by the MCMC algorithm holds exactly for all sources. Thus, any imperfections in the real data, such as intrinsic scatter, are not taken into account. We discuss the addition of intrinsic sidedness in Section 3.2. The simulated sample and real data are shown overplotted in Fig. 2(a).

3.2 Including the intrinsic sidedness

We modelled the jets as described in Section 3.1, but allowed values of k to be drawn from the ratio of two truncated Gaussian distributions of full width half maximum (FWHM) derived from the data. Fitting the data as above, we obtained a jet speed of $\beta = 0.5 \pm 0.2$ with the best-fitting σ of the Gaussians from which k was drawn equal to 0.4 ± 0.2 . The errors quoted here are derived from simula-



(a)



(b)

Figure 2. The simulated data (dashed lines) over-plotted on the sample data (solid lines). The simulated sample shown in Fig. (a) includes no intrinsic sidedness and uses a best fit jet speed of $(0.60 \pm 0.02)c$. Fig. (b) shows the results of including some intrinsic sidedness in the distribution, with a best fitting $\beta = 0.5 \pm 0.2$, as described in the text.

tions as in Section 3.1. The data and simulated sample are shown in Fig. 2(b).

4 DISCUSSION

4.1 Are WAT jets beamed?

The jet speeds with no intrinsic scatter for WAT sources obtained by Hardcastle & Sakellou (2004) and O'Donoghue et al. (1990) are lower than found here (but within our errors), but the sample used here is larger, and we have not preferentially selected sources with jet sidedness close to unity; inadvertent selection of sources with sidedness values close to unity has hampered previous studies. Comparing our results to jet speeds obtained for both FRI and FRII type sources, it appears that the jet speed results presented here for

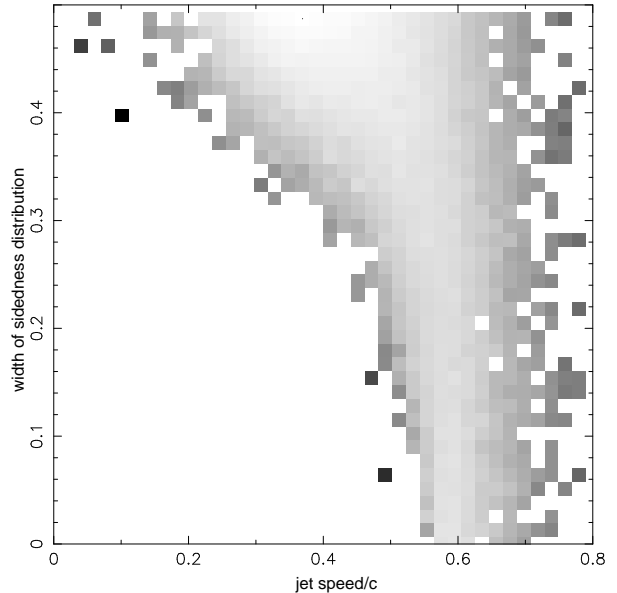


Figure 3. A plot showing the relative likelihood of the different pairs of jet speed and jet sidedness values that were fitted to the data. The grey-scale indicates the likelihood of each combination, with the darkest grey representing those values that are the least likely, and the lightest shades of grey representing the most likely. The unshaded areas show regions of the parameter space that were not sampled, as they were not expected to yield sensible fits. There is very little difference between the likelihood of a model with some intrinsic scatter and some beaming, and one with less beaming where intrinsic sidedness determines the distribution. For clarity, whilst the actual parameter space investigated is larger than that shown, we restrict this plot to the region of parameter space with $\sigma < 0.5$ and $\beta < 0.8$.

WAT sources are consistent with mean jet speeds found for FRI radio sources, at the points where FRI jets flare ($(0.54 \pm 0.03)c$ (Arshakian & Longair 2004, and references therein)). Using different samples and analysis methods, Arshakian & Longair (2004), Hardcastle et al. (1999) and Wardle & Aaron (1997) find speeds in FRII jets in the range $0.5 - 0.7c$, which are also consistent with the jet speeds found in WATs.

There is however, a fundamental degeneracy between the beaming speed and intrinsic scatter, since we cannot, *a priori*, rule out a model that contains no beaming, but has just the right amount of intrinsic sidedness to reproduce the observed distribution. However, since models with and without intrinsic scatter require some beaming, it is likely that jets in WATs are at least mildly relativistic, with the beaming speed obtained in this study being an upper limit, as intrinsic sidedness reduces the required beaming speed.

Orr & Browne (1982) show that as the core of a radio galaxy is essentially the unresolved bases of the two relativistic jets, the radio core should show some evidence for beaming; the core prominence distribution for a sample of sources, i.e. the distribution of the ratios of the flux of the beamed core to the flux from the unbeamed components, should be dependent on the jet speed. Therefore, as the jet sidedness distribution is also a function of jet speed, jet sidedness and core prominence should show some correlation. However, a plot of these two quantities (Fig. 4) shows at best a weak correlation. It would appear that despite the jet speeds found in Sections 3.1 and 3.2, the cores in these sources show only marginal evidence for beaming. This could simply indicate that core prominence is not a good indicator of beaming in these sources, as the jet

sidedness ratios do indicate that at least some relativistic beaming is present.

The use of core prominence as a beaming indicator relies on the hypothesis that the beamed and unbeamed components of a radio source are always identical; the only difference between different radio sources is the angle that the jets make with the line of sight. If this is not the case, then there will be scatter in the relationship between jet-sidedness and core prominence, as they will not be measuring the same thing. The extended emission in WATs should be dominated by old material flowing down the lobes. Therefore, we expect that the ratio of the unbeamed to the beamed flux of a given source will depend on the age of the source, weakening the relationship between core prominence and jet sidedness, as an older source may still be beamed, but due to a large amount of old material in the lobes, have a small core prominence. This age dependence of unbeamed flux, combined with the scatter in jet speed, could lead to the core prominence being an unreliable indicator of beaming in WAT sources.

Given that some WAT sources exhibit hotspot like features (Hardcastle & Sakelliou 2004), it would be surprising if at least some relativistic beaming were not responsible for the observed sidedness distribution. If the hotspots in WATs are analogous to FRII hotspots, this implies that WAT hotspots are jet termination shocks. If that is the case, then the hotspots indicate that the jet is faster than the internal sound speed ($c/\sqrt{3}$ for a relativistic plasma). Since hotspots are not a universal feature of WATs, it would appear that the jet speed in WATs could be approximately the internal sound speed of the jets (compare $0.60 \pm 0.02c$ above for jets with no intrinsic variance, with $0.58c$ as the internal sound speed in a relativistic plasma), with intrinsic variation in the jet speed accounting for the presence or absence of hotspots. If this is the case, then it would be expected that approximately half of the sources in the sample would show hotspots, and half would not. As high resolution data is required in order to ascertain the presence of a hotspot, the Hardcastle & Sakelliou (2004) sample, which is a sub-sample of the one presented in this paper, was examined to obtain the proportion of plumes with and without hotspots. A plume was categorised as having a hotspot if it contained a bright, compact structure, coincident with the termination point of a jet. If there was bright, compact structure in the plume, but the end of the jet could not be traced into the plume, the region was classified as a possible hotspot. In that sample we find that 5 plumes contain definite hotspots, 5 plumes do not contain hotspots, and 4 plumes contain bright, reasonably compact structures in the plumes, that could be associated with jet termination (possible hotspots). This is consistent with the suggestion that intrinsic variation in speed could account for the presence or absence of hotspots in WAT sources.

4.2 Jet bending in WATs

As seen in Hardcastle & Sakelliou (2004), most WAT jets show some slight bending of the jets. It can be argued that very light, very relativistic jets should be ‘stiff’ and resistant to bending, requiring unreasonably high host galaxy speeds. However, if the jets are moderately relativistic, as has been argued in Section 4.1, then more reasonable galaxy speeds should be required, provided that the jets are light. Following the discussion of jet bending in Hardcastle et al. (2005), an estimate of the maximum velocity of the host galaxy can be made. We use Euler’s equation in the form

$$\frac{\rho_j v_j^2}{R} = \frac{\rho_{\text{ext}} v_g^2}{h_j} \quad (3)$$

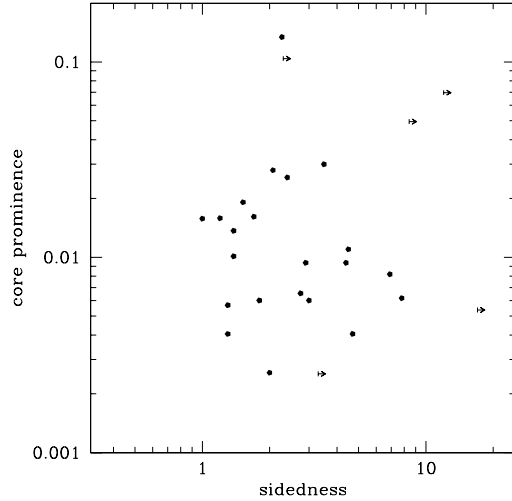


Figure 4. Core prominence plotted against jet sidedness for our WATs sample. The arrows show those points for which limits for jet-sidedness were obtained.

(e.g. O’Dea 1985) where ρ_j is the density of the jet, v_j is the speed of the jet, R is the radius of curvature of the jet, ρ_{ext} is the density of the inter-galactic medium, and h_j is the width of the jet. We assume a jet speed of $0.6c$, and as in Hardcastle et al. (2005) we take the minimum equivalent external density to be given by $\rho_j = 3p_{\text{min}}/c^2$ where p_{min} is the minimum internal pressure of the jet. Using a proton number density (n_p) of 1500 m^{-3} , and the minimum internal pressure of the jet to be $3 \times 10^{-12} \text{ Pa}$ (from Hardcastle et al. 2005), a galaxy speed of 140 km s^{-1} is needed to produce a bend in the jet of 3C465 of one jet width, which is the most that the jets in 3C465 appear to bend over their lengths. This galaxy speed is plausible for a large central galaxy sitting in the centre of X-ray emission from a cluster, as 3C465 does, and given that the estimate of ρ_j is a lower limit, it seems likely that small scale jet bending can occur in WATs in clusters, if the jet is light.

In addition to WAT sources that have mainly straight jets, with only small bends, there is also a class of radio galaxies that whilst exhibiting classical WAT morphology, also have extremely bent inner jets; the best example of this class of source is 0647+693 (Hardcastle & Sakelliou 2004), but other sources with a similar morphology are shown in Appendix A (e.g. 2151+085). If the jet speeds are as fast as we have deduced here, and we assume that, as in 3C465 above, the jet bending is caused by the bulk motions of the host galaxy through the IGM, we can ask whether the galaxy velocity is plausible for a galaxy sitting at or near the centre of a cluster.

To induce bending of the scale seen in 0647+693, where the distance from the core to the base of the plume is 30 arcsec (Hardcastle & Sakelliou 2004), and the jet bends by 20 arcsec over the length of the jet, higher speeds are required. Assuming that the jets in 0647+693 have a similar density to those in 3C465, and that the cluster environment of 0647+693 is similar to that of 2236-176 (Jetha et al. 2005) as the temperatures are reasonably similar, the electron number density (n_e) at the base of the plume in 0647+693 (30 kpc from the radio core) is approximately 1500 m^{-3} . Further assuming that the proton number density, $n_e = 1.18n_p$, an external density at the base of the plumes of $2.13 \times 10^{-24} \text{ kg m}^{-3}$ is obtained. Assuming that $h_j \sim 1 \text{ arcsec}$, the jet bends by approxi-

mately 20 jet widths before the jet enters the base of the plume. Using Eqn. 3, a galaxy speed of 870 km s^{-1} is needed to bend the jets on the scales seen. This velocity is rather high for a galaxy near the centre of a cluster, but, if the cluster had undergone a recent merger event, this velocity would certainly be plausible, suggesting that WATs with bent jets could be tracing a recent cluster merger event. The velocities required to bend the jets also provide evidence for a model in which the jets are relativistic but light; jets with densities much higher than the minimum inferred densities would require much larger velocities to bend.

The same host galaxy speed must also bend the plumes (e.g. Eilek et al. 1984). Since the plumes, on average, tend to be more bent than the jets in WATs, this implies that the flow in the plumes is significantly different to the flow in the jets. It is already established that whilst WAT jets may be one-sided, WAT plumes are always two-sided (3C465 is a good example of this behaviour Hardcastle et al. 2005). This points to the flow in the plumes being substantially slower than that in the jets, such that the jets may be beamed as discussed in this paper, but the plumes certainly will not be. This implies that the deceleration of WAT jets may be quite sudden, and is consistent with observations showing a hotspot-like feature at the jet termination point.

5 CONCLUSIONS

We have presented a sample of 30 WATs that we have used to obtain a representative jet speed for WAT jets. If we assume that there is no beaming, then the observed distribution can be reproduced with some (large) amount of intrinsic sidedness in the jets. However, if we assume that the observed sidedness distribution is due to beaming coupled with some sensible moderate intrinsic distribution, then we obtain a jet speed in the range $(0.3 - 0.7)c$. Whilst the sidedness analysis of the kpc-scale jets in our WAT sample alone cannot confirm these jet speeds, comparisons with the jet speeds of FRI and FRII sources suggests that moderate beaming is at least necessary. Further, if we assume that the jets are fast, then our jet bending analysis in Section 4.2, supports the hypothesis that jets in WATs are light so that they can be bent through the angles seen in sources such as 0647+693 whilst requiring reasonable galaxy speeds.

The arguments presented in Section 4.1 outline why core prominence may not be a reliable indicator of beaming in WAT sources, and this could explain why the correlation between jet-sidedness and core prominence is weak in this sample of sources.

Studies of FRI and FRII radio galaxies have established the relativistic nature of the jets in these sources by examining the nature of the pc-scale jets, and it is thought that any sidedness that exists on the pc-scale will persist to the kpc-scale, if the kpc-scale jets are relativistic. By examining the pc-scale jets of WATs it could be established whether the pc-scale jets are relativistic, and if this persists in the kpc-scale jets. Some studies of the jets in WAT sources have been done (e.g. for 3C465 and 0836+290 Venturi et al. 1995 and Giovannini et al. 2001) where one-sided pc-scale jets are found that are well aligned with the kpc-jets. No proper motions are found as yet, but from these two objects, it would seem that the one-sidedness persists from pc to kpc-scale. This implies that if the pc-scale jet is beamed, then the kpc-scale jet must also be beamed. A larger investigation of the pc-scale jets in for example, the sample of WATs presented here, would enable us to establish whether the sidedness persists on pc and kpc-scales for all sources, or just for some. This would allow the jet speeds to be further constrained.

ACKNOWLEDGEMENTS

NNJ thanks PPARC for a research studentship. MJH thanks the Royal Society for a research fellowship. IS acknowledges the support of the European Community under a Marie Curie Intra-European Fellowship. We thank Mike Hobson for the use of his METRO MCMC sampler and the referee for helpful comments that were useful in improving the paper. The National Radio Astronomy Observatory is a facility of the National Science Foundation operated under cooperative agreement by Associated Universities, Inc.

REFERENCES

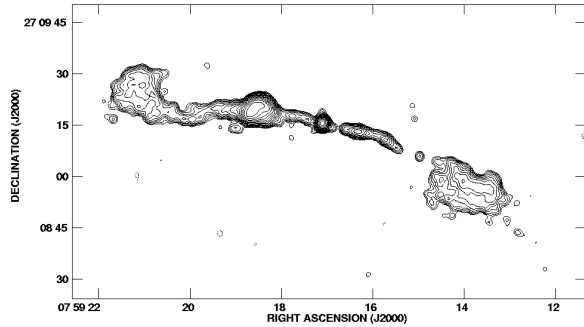
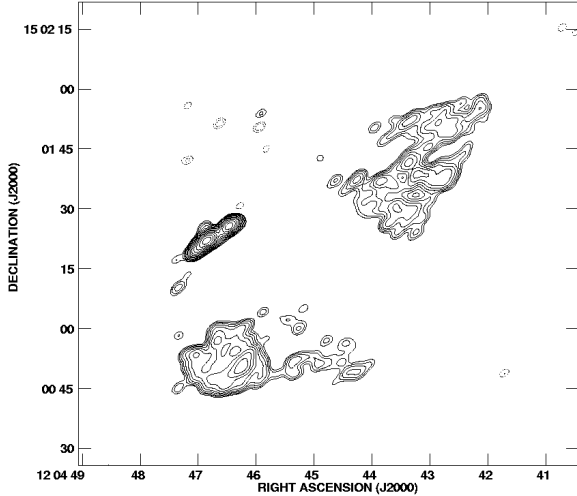
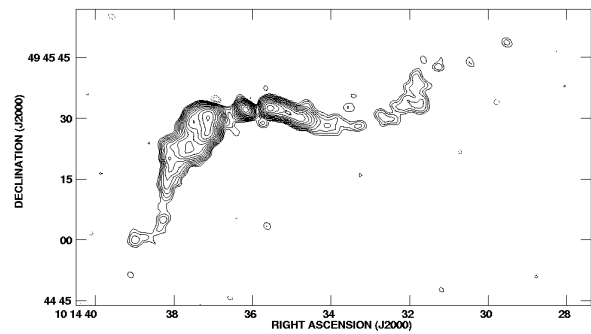
Arshakian T. G., Longair M. S., 2004, MNRAS, 351, 727
 Eilek J. A., Burns J. O., O'Dea C. P., Owen F. N., 1984, ApJ, 278, 37
 Fanaroff B. L., Riley J. M., 1974, MNRAS, 167, 31
 Giovannini G., Cotton W. D., Feretti L., Lara L., Venturi T., 2001, ApJ, 552, 508
 Hardcastle M. J., 1999, A&A, 349, 381
 Hardcastle M. J., Alexander P., Pooley G. G., Riley J. M., 1999, MNRAS, 304, 135
 Hardcastle M. J., Sakelliou I., 2004, MNRAS, 349, 560
 Hardcastle M. J., Sakelliou I., Worrall D. M., 2005, MNRAS, 359, 1007
 Hobson M. P., Baldwin J. E., 2004, Applied Optics, 43, 2651
 Jetha N. N., Sakelliou I., Hardcastle M. J., Ponman T. J., Stevens I. R., 2005, MNRAS, 358, 1394
 Laing R. A., Parma P., de Ruiter H. R., Fanti R., 1999, MNRAS, 306, 513
 Ledlow M. J., Owen F. N., 1995, AJ, 110, 1959
 Lind K. R., Blandford R. D., 1985, ApJ, 295, 358
 Mullin L., et al., in prep
 O'Dea C. P., 1985, ApJ, 295, 80
 O'Donoghue A. A., Eilek J. A., Owen F. N., 1990, ApJS, 72, 75
 Orr M. J. L., Browne I. W. A., 1982, MNRAS, 200, 1067
 Owen F. N., Ledlow M. J., 1997, ApJS, 108, 41
 Venturi T., Castaldini C., Cotton W. D., Feretti L., Giovannini G., Lara L., Marcaide J. M., Wehrle A. E., 1995, ApJ, 454, 735
 Wardle J. F. C., Aaron S. E., 1997, MNRAS, 286, 425

APPENDIX A: NEW RADIO MAPS OF WATS

As discussed in Section 2, new data for some of our sample were obtained, in order to enlarge the WATs sample, where no good quality data were available. Here we present the new radio maps obtained during our VLA observing programme (Figs A1 - A9). We also present some previously unpublished maps from data taken from the VLA archive. In Table A1 we show the details of the observations used to make the maps presented here.

Table A1. Details of observations for which new maps are presented in Appendix A

Abell cluster	radio name (B1950)	array configuration	observation frequency (GHz)	time on source (min)	observation date	map resolution (arcsec×arcsec)	VLA proposal number
A610	0756+272	C	8.5	39	2004-MAR-30	2.20×2.05	AJ309
A950	1011+500	C	8.5	39	2004-MAR-30	2.56×2.03	AJ309
A1462	1202+153	C	8.5	39	2004-MAR-30	3.63×2.21	AJ309
		C	8.5	28	2004-APR-26		AJ309
A1529	1221+615	C	8.5	39	2004-MAR-30	2.68×1.74	AJ309
		C	8.5	29	2004-APR-26		AJ309
A1667	1300+321	C	8.5	39	2004-MAR-30	2.98×2.27	AJ309
A2225	1638+558	BC	8.5	48	2004-FEB-2	3.39×2.02	AJ309
		C	8.5	31	2004-APR-26		AJ309
A2249	1707+344	BC	8.5	45	2004-FEB-2	2.91×1.94	AJ309
		C	8.5	31	2004-APR-26		AJ309
A2395	2151+085	BC	8.5	47	2004-FEB-2	2.22×2.06	AJ309
A2617	2330+091	BC	8.5	48	2004-FEB-2	2.07×2.02	AJ309
A1446	1159+583	B	4.86	125	1984-FEB-17	1.29×1.06	AO049
A2029	1508+059	A	8.5	367	1992-NOV-14	0.29×0.26	AT144
		B	8.5	151	1993-MAR-24		
A1684	1306+107A	B	4.86	136	1985-DEC-07	13.25×11.88	AO062
A194	3C40	B	1.5	335	1984-JAN-08	5.58×5.17	AV102
		C	1.5	206	1984-JUN-02		AV102
		D	1.5	81	1984-JUL-31		AV112

**Figure A1.** 8-GHz, 2.20×2.05-arcsec resolution radio map of 0756+272, hosted by the cluster Abell 610. Contours are in logarithmic $\sqrt{2}$ steps, with the lowest contour being at 0.25mJy/beam**Figure A3.** 8-GHz, 3.63×2.21-arcsec resolution radio map of 1202+153, hosted by the cluster Abell 1462. Contours are as Fig A1, with the lowest contour being at 0.35mJy/beam**Figure A2.** 8-GHz, 2.56×2.03-arcsec resolution radio map of 1011+500, hosted by the cluster Abell 950. Contours are as Fig A1, with the lowest contour being at 0.38mJy/beam

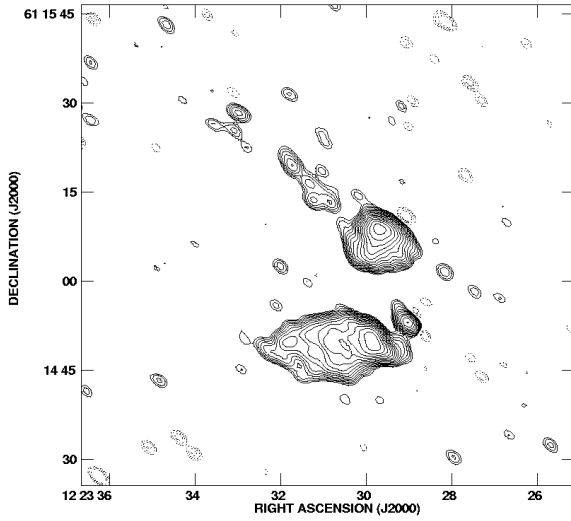


Figure A4. 8-GHz, 2.68×1.74 -arcsec resolution radio map of 1221+615, hosted by the cluster Abell 1529. Contours are as Fig A1, with the lowest contour being at 0.47mJy/beam

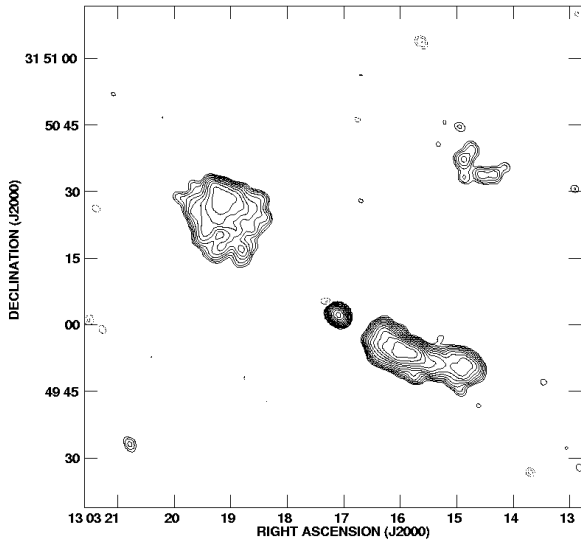


Figure A5. 8-GHz, 2.98×2.27 -arcsec resolution radio map of 1300+321, hosted by the cluster Abell 1667. Contours are as Fig A1, with the lowest contour being at 1.4mJy/beam

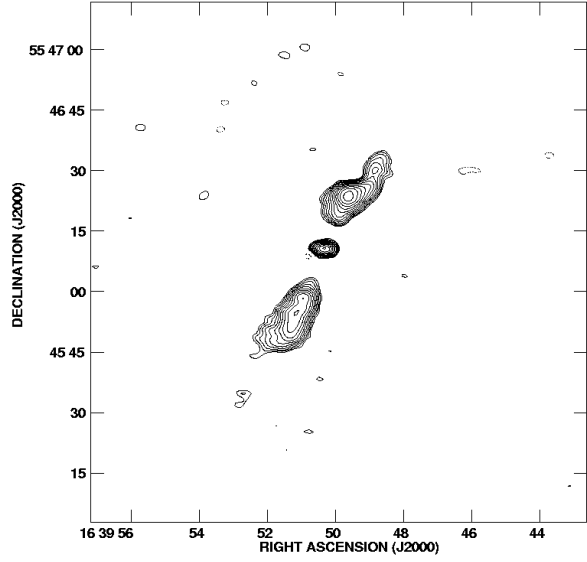


Figure A6. 8-GHz, 3.39×2.02 -arcsec resolution radio map of 1638+558, hosted by the cluster Abell 2225. Contours are as Fig A1, with the lowest contour being at 0.012mJy/beam. Whilst we cannot detect the jets in this source, it is still part of the WAT sample, but was not used in the jet-speed analysis.

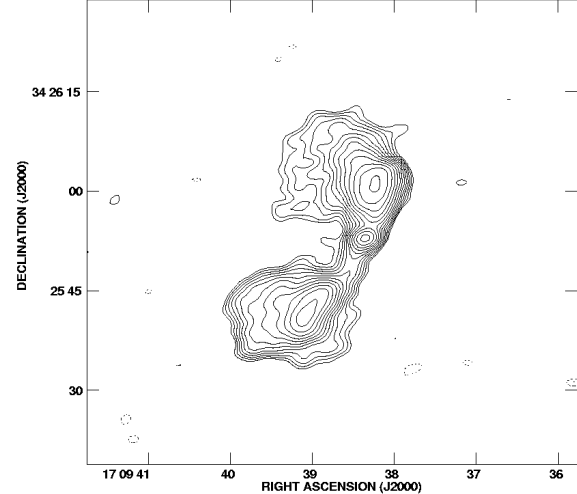


Figure A7. 8-GHz, 2.91×1.94 -arcsec resolution radio map of 1707+344, hosted by the cluster Abell 2249. Contours are as Fig A1, with the lowest contour being at 0.20mJy/beam

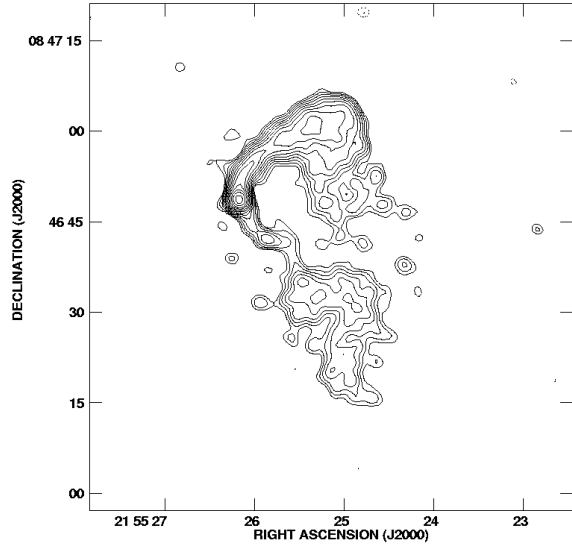


Figure A8. 8-GHz, 2.22×2.06 -arcsec resolution radio map of 2151+085, hosted by the cluster Abell 2395. Contours are as Fig A1, with the lowest contour being at 0.080mJy/beam

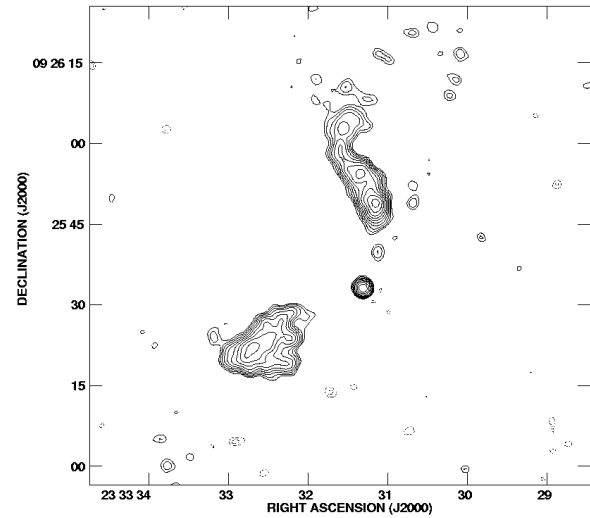


Figure A9. 8-GHz, 2.07×2.02 -arcsec resolution radio map of 2330+091, hosted by the cluster Abell 2617. Contours are as Fig A1, with the lowest contour being at 0.073mJy/beam. Whilst we cannot detect the jets in this source, it is still part of the WAT sample, but was not used in the jet-speed analysis.

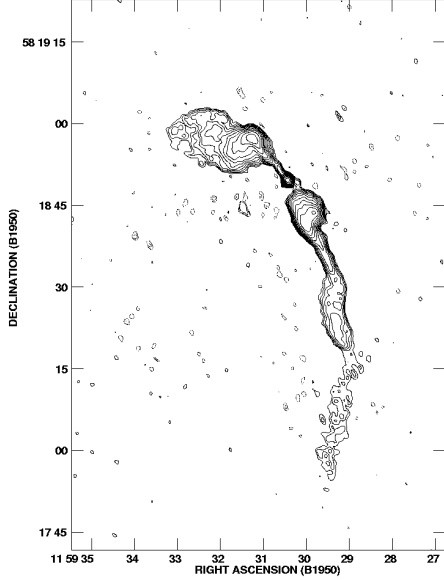


Figure A10. 4.86-GHz, 1.29×1.06 -arcsec resolution radio map of 1159+583, hosted by the cluster Abell 1446. Contours are as Fig A1, with the lowest contour at 0.13mJy/beam. The map was made with data obtained from the VLA archive

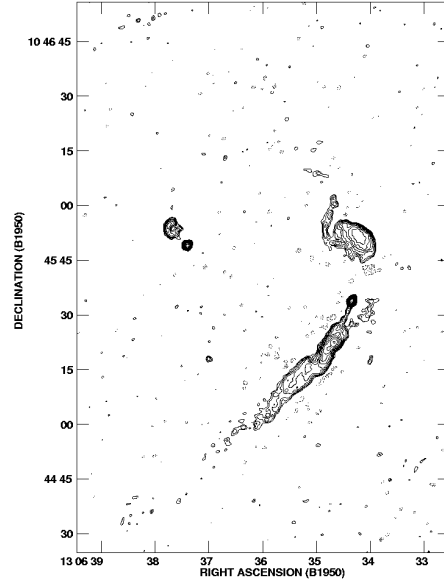


Figure A11. 4.86-GHz, 1.29×1.06 -arcsec resolution radio map of 1306+107A, hosted by the cluster Abell 1684. Contours are as Fig A1, with the lowest contour at 0.10mJy/beam. The map was made with data obtained from the VLA archive

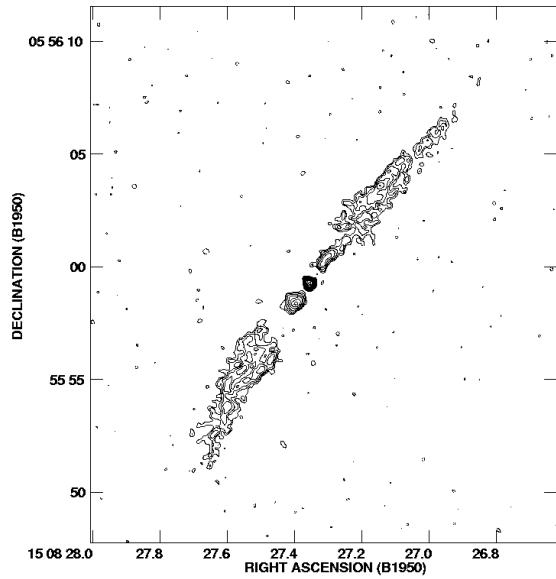


Figure A12. 8.0-GHz, 0.29×0.26 -arcsec resolution radio map of 1508+059, hosted by the cluster Abell 2029. Contours are as Fig A1, with the lowest contour at 0.054mJy/beam. The map was made with data obtained from the VLA archive

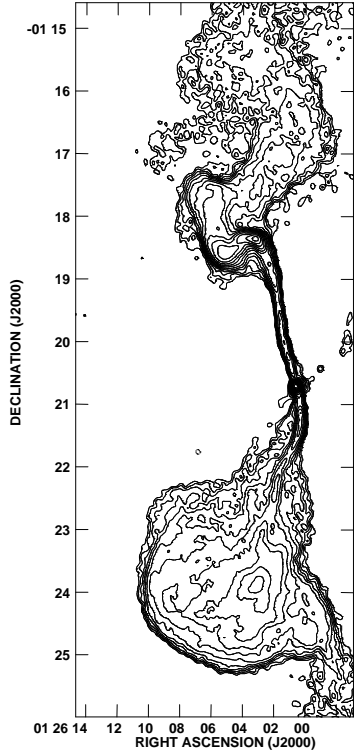


Figure A13. 1.5-GHz, 5.58×5.17 -arcsec resolution radio map of 3C40, hosted by the cluster Abell 194. Contours are as Fig A1, with the lowest contour at 0.40mJy/beam. The map was made with data obtained from the VLA archive